

AUGER RECOMBINATION IN ANTIMONY-BASED, STRAIN-BALANCED, NARROW-BAND-GAP SUPERLATTICES

J.T. OLESBERG*, THOMAS F. BOGGESS*, S.A. ANSON*, D.-J. JANG*, M.E. FLATTÉ*, T.C. HASENBERG*, C.H. GREIN**

* Department of Physics and Astronomy, University of Iowa, Iowa City, IA 52242

** Department of Physics, University of Illinois, Chicago, IL 60607

ABSTRACT

Time-resolved all-optical techniques are used to measure the density and temperature dependence of electron-hole recombination in an InAs/GaInSb/InAs/AlGaInAsSb strain-balanced superlattice grown by molecular beam epitaxy on GaSb. This 4 μm bandgap structure, which has been designed for suppressed Auger recombination, is a candidate material for the active region of mid-infrared lasers. While carrier lifetime measurements at room temperature show unambiguous evidence of Auger recombination, the extracted Auger recombination rates are considerably lower than those reported for bulk materials of comparable bandgap energy. We find that the Auger rate saturates at carrier densities comparable to those required for degeneracy of the valence band, illustrating the impact of Fermi statistics on the Auger process. The measured results are compared with theoretical Auger rates computed using a band structure obtained from a semi-empirical 8-band $\mathbf{K}\cdot\mathbf{p}$ model. We find excellent agreement between theoretical and experimental results when Umklapp processes in the growth direction are included in the calculation. Measured recombination rates from 50 to 300 K are combined with calculated threshold carrier densities to determine a material T_0 value for the superlattice.

INTRODUCTION

Auger recombination is one of the main factors limiting operation of mid-infrared semiconductor lasers. One strategy for minimizing Auger recombination is to utilize semiconductors with large type-II band offsets in the design of materials with a small band-edge density of states and minigaps in the band structure one band gap from the band edges. It is important to experimentally verify the extent to which Auger suppression is achieved in these designs. Comparison of measured and calculated Auger rates also provides a stringent test of the accuracy of band structure and matrix element calculations used in theoretical optimization of material properties.

EXPERIMENT

The structure under investigation was grown for optical characterization measurements using a Perkin-Elmer 430P MBE machine on a nominally undoped GaSb substrate. A schematic of the epitaxial structure is shown in Figure 1(a). Forty periods of a four-layer superlattice are grown between AlGaInAsSb barriers. The barriers serve to increase the absorption of the optical excitation source and keep the photogenerated carriers in the superlattice. Figure 1(b) shows one period of the superlattice. Room temperature photoluminescence from this structure indicates a band gap near 4.0 μm and good structural quality. A four-layer superlattice using the same alloys but with slightly different layer thicknesses has been described earlier.¹ An optically-pumped 5.2 μm laser using a similar superlattice has operated at 185 K.²

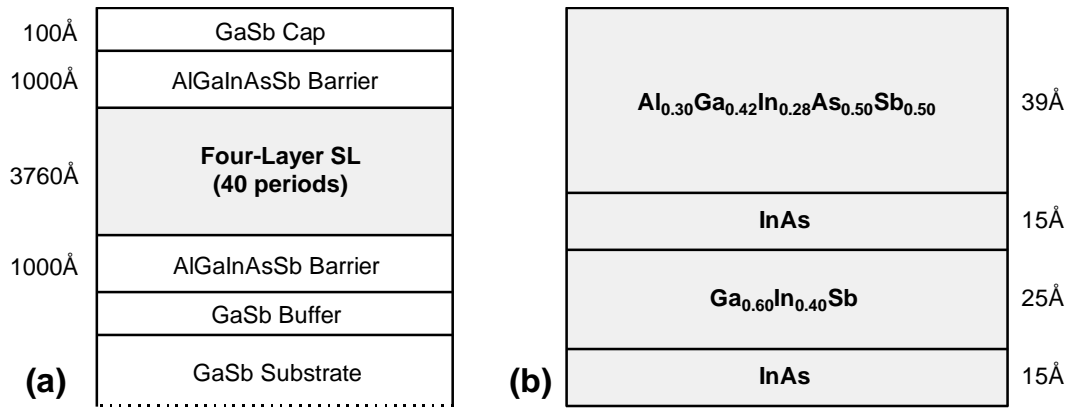


Figure 1: (a) Schematic of the epitaxial structure of the sample and (b) schematic of one period of the four-layer superlattice.

Two optical methods have been used to measure recombination rates in this sample: time-resolved differential transmission³ and time-resolved photoluminescence upconversion.⁴ A schematic of the differential transmission measurement is shown in Figure 2(a). A pulse from a Ti:sapphire laser is used to create a dense distribution of nonequilibrium carriers in the sample. The transmission of the sample is then probed with the mid-infrared output of an optical parametric oscillator.⁵ The wavelength of the mid-infrared probe is tunable from 2.6 - 4.4 μm .⁶ After passing through the sample, the probe is directed through a monochromator which increases the spectral resolution of the measurement. The transmitted probe intensity is measured with a liquid nitrogen cooled InSb detector. By chopping the pump and probe separately, we can extract a signal proportional to the change in transmission of the probe induced by the non-equilibrium carriers and a signal proportional to the equilibrium transmission of the probe. These values are used to calculate the differential transmission, which is the change in transmission induced by the presence of the non-equilibrium carriers normalized by the equilibrium transmission.

A schematic of the time-resolved photoluminescence upconversion experiment is shown in Figure 2(b). Each pulse from the Ti:sapphire laser is split into two. One is used to excite the sample, which is mounted in a variable temperature dewar. The mid-infrared photoluminescence from the sample is collected and imaged onto a nonlinear crystal. The remaining portion of the

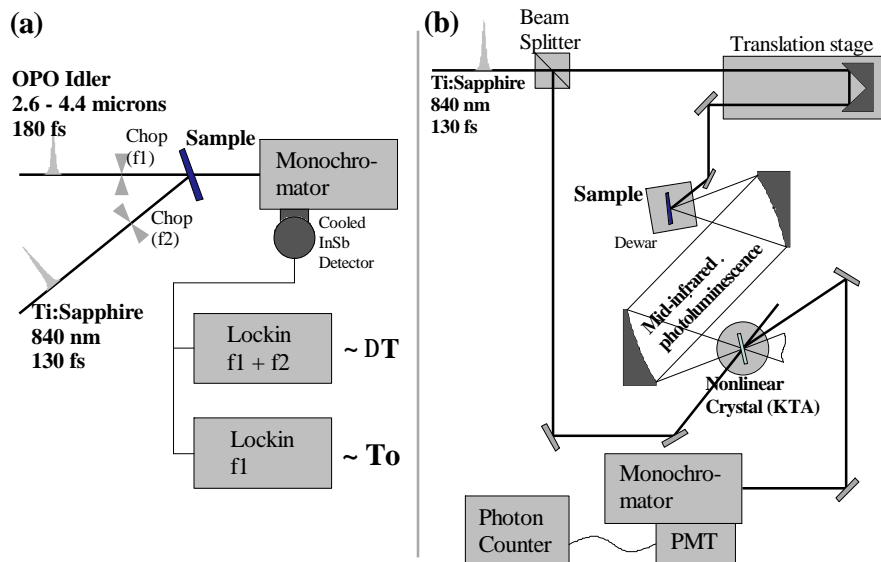


Figure 2: (a) Schematic of the differential transmission experiment. (b) Schematic of the time-resolved photoluminescence upconversion experiment.

Ti:sapphire pulse is focused onto the same spot on the nonlinear crystal. A portion of the mid-infrared photoluminescence is upconverted to visible wavelengths and directed into a monochromator and photon-counted using a photomultiplier tube. The measured signal is the intensity of the upconverted photoluminescence, which is proportional to the intensity of the original mid-infrared photoluminescence. The temporal resolution in this experiment comes from the sum frequency generation: the Ti:sapphire pulse involved in the upconversion process acts as a temporal gate. In both experiments, the temporal resolution is approximately 200 fs.

Recombination rates (the inverse of the instantaneous lifetime) are extracted from the data using

$$R = \frac{1}{N} \frac{dN}{dt} = \frac{1}{N} \frac{\mathcal{I}N}{\mathcal{I}(\text{Signal})} \frac{d(\text{Signal})}{dt} \quad (1)$$

where R is the recombination rate per carrier, N is the carrier density, and “*Signal*” is either differential transmission or upconverted photoluminescence intensity. We assume that the initial carrier density in our superlattice is uniform over the length of the structure and that it is proportional to the incident photon density. The first assumption is reasonable since the carriers are injected with almost 1 eV of excess energy and will be able to distribute themselves throughout the superlattice before cooling to the band edge. The second assumption is necessary to avoid the very difficult process of modeling the density and excess energy dependent capture properties of the superlattice.

Since the photoexcited carriers are created with a large excess energy, it is expected that some will escape into the substrate before cooling to the band edge of the superlattice. Thus the photoexcited carrier density calculated using the pump photon density, pump absorption coefficient, and sample thickness represents an upper limit of the true carrier density in the superlattice. In the pump-probe experiment, we can also calculate the carrier density in the superlattice by comparing the saturation of the experimental differential-transmission with the calculated saturation due to the $(1 - f_e - f_h)$ term in the density-dependence of the absorption coefficient at the probe wavelength. In the photoluminescence-upconversion experiment, we can calculate the carrier density by comparing the widths of the measured and calculated photoluminescence spectra. All three methods are in reasonable agreement and we estimate the uncertainty in the density to be on the order of 25%.

RESULTS

Recombination rates at 300K are shown as a function of density in Figure 3(a). From the zero density intercept, we can extract a Shockley-Read-Hall rate corresponding to a lifetime of 2.7 ns. This is a characteristic lifetime for good quality structures grown in this MBE machine. The calculated transparency density for the superlattice is indicated in the figure. This gives a lower bound on the densities of interest for laser operation. At material transparency, the total recombination rate is just over 1 ns^{-1} (a lifetime of 0.95 ns). We expect radiative recombination to be insignificant in this structure at all but the lowest densities due to the type-II nature of the superlattice. Calculations of the radiative recombination rate show it to be more than a factor of 30 smaller than the total recombination rate for all densities considered at 300 K.

The total recombination rate increases nearly quadratically ($R \approx A + CN^2$ for $BN \ll A + CN^2$, where A , B , and C are the Shockley-Read-Hall, Radiative, and Auger coefficients, respectively) with density for densities below $9 \times 10^{17} \text{ cm}^{-3}$, but becomes sub-quadratic

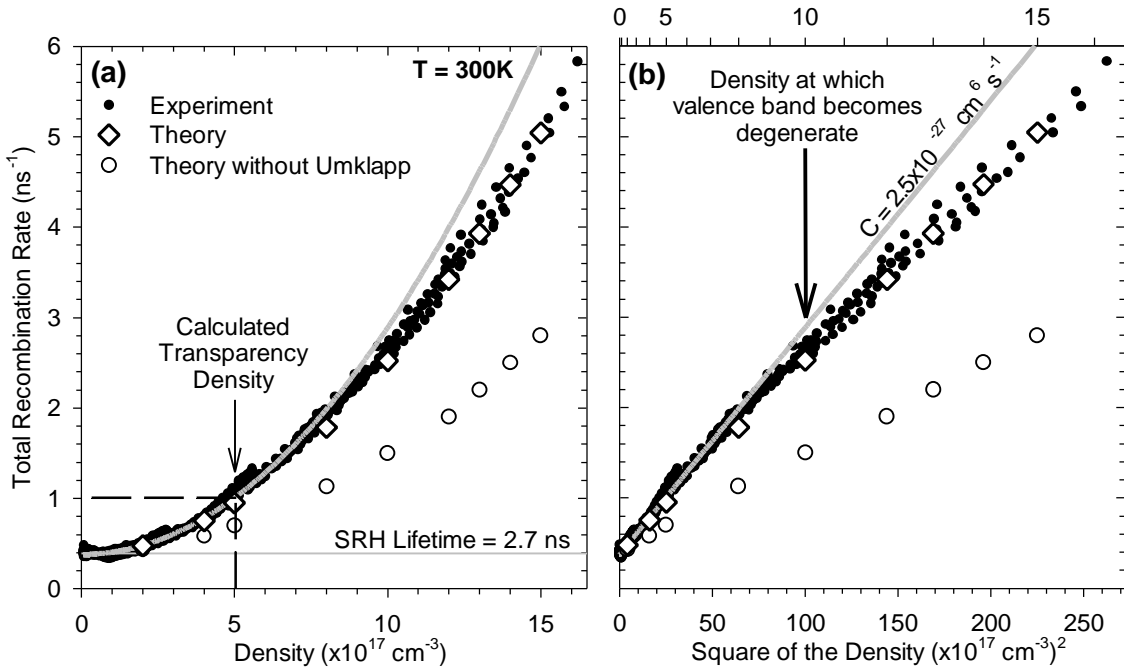


Figure 3: (a) Room temperature recombination rate as a function of density. (b) Recombination rate as a function of the square of the density.

at higher densities. The sub-quadratic dependence can be seen more clearly in Figure 3(b) where the recombination rate is shown as a function of the square of the density. On this figure, quadratic density-dependence appears as a straight line. The recombination rates lie on a straight line at low densities (up to approximately $9 \times 10^{17} \text{ cm}^{-3}$), from which an Auger coefficient of $2.5 \times 10^{-27} \text{ cm}^6 \text{ s}^{-1}$ is extracted (the solid line in Figure 3(a) is the same as that in Figure 3(b)). This value of the Auger coefficient is approximately four times smaller than the value of $11 \times 10^{-27} \text{ cm}^6 \text{ s}^{-1}$ measured in InAs.⁷ In light of the fact that the superlattice being studied has a bandgap 40 meV smaller than that of InAs, the measured Auger coefficient indicates that the Auger optimizations performed on this sample have been successful.

Sub-quadratic density-dependence of the Auger rate has previously been experimentally observed in bulk InSb.⁸ Quadratic density-dependence is appropriate only for nondegenerate bands. The transition to sub-quadratic behavior is a consequence of Fermi statistics on the Auger process. The fact that we observe the transition to sub-quadratic behavior at densities very close to those at which the valence band becomes degenerate implies that Auger recombination in our system is dominated by hole-hole processes.

Auger rates for this structure have been calculated using band structures and momentum-dependent matrix elements calculated using 8-band superlattice $\mathbf{K} \cdot \mathbf{p}$ theory.⁹ The accuracy of the band structure and matrix element calculation has been verified experimentally with a different type-II structure.¹⁰ The results of the theoretical calculations are shown in Figure 3 along with the experimental data. There are no adjustable parameters used in the theoretical calculation. The experimental Shockley-Read-Hall rates have been added to the theoretical Auger rates to simplify comparison. The agreement between the experimental measurements and theoretical calculations is excellent given the difficulty of both the experiment and calculation. Theory and experiment are in agreement in both the magnitude and the density dependence of the Auger rate.

Figure 4(a) shows the measured and calculated Auger rates as a function of lattice temperature for three densities. The experimental Auger rate is extracted from the data by subtracting the experimental Shockley-Read-Hall rate and the calculated radiative rate from the

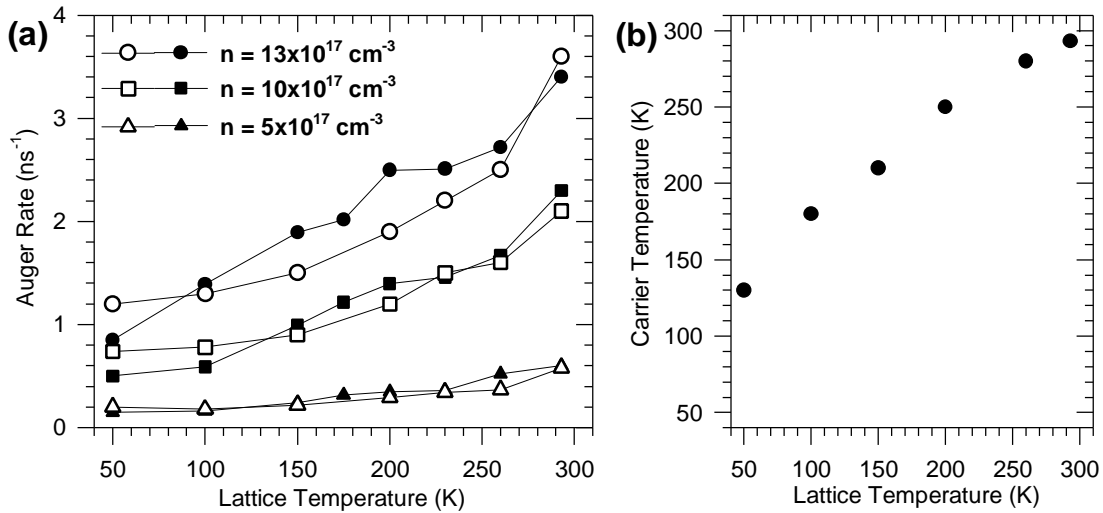


Figure 4: (a) Measured (solid symbols) and calculated (hollow symbols) Auger rates as a function of temperature. The lines connecting the calculated points are merely a guide to the eye. (b) Average carrier temperature as a function of lattice temperature.

data. The calculated radiative rate is less than 20% of the total rate at all densities and temperatures. Both theory and experiment show increasing Auger rates at increasing temperature. Again, the agreement between theory and experiment is very good.

Figure 4(b) shows the average carrier temperature corresponding to the different lattice temperatures in the measurement. The carrier temperature was determined by fitting the high-energy tail of the upconverted photoluminescence spectra to a Boltzmann distribution. Since the Auger rate is strongly dependent on the carrier temperature, the experimental carrier temperatures were used in the calculation of the Auger rates. The shown temperature is the average carrier temperature over the interval from 10 ps - 1 ns.

The measured recombination rates can be used to calculate threshold current densities for this material. In Figure 5, threshold current density is shown as a function lattice temperature for a range of material gains. The density required for a given amount of gain is taken from absorption calculations. However, the gain has been scaled with experimental data from the differential transmission experiment and is thus semi-empirical. From the temperature dependence of the injected current densities, we calculate a material T_0 of 78 K for transparency and 69 K for 500 cm⁻¹ of gain. These values of T_0 are for the superlattice material. The T_0 for a device which utilizes this superlattice as the active region will likely be smaller since there are additional temperature-dependent effects in a real device which are not present in our optical tests (e.g., leakage current).

CONCLUSIONS

We have measured recombination rates as a function of density and temperature in a narrow-bandgap superlattice designed to suppress Auger recombination. At low densities, the room temperature Auger coefficient is $C = 2.5 \times 10^{-27} \text{ cm}^6 \text{ s}^{-1}$. Excellent agreement is demonstrated between measured and calculated Auger recombination rates for all temperatures and densities considered. Temperature-dependent current densities have been determined. For 500 cm⁻¹ of material gain, the superlattice has a characteristic temperature of 69 K. The small room

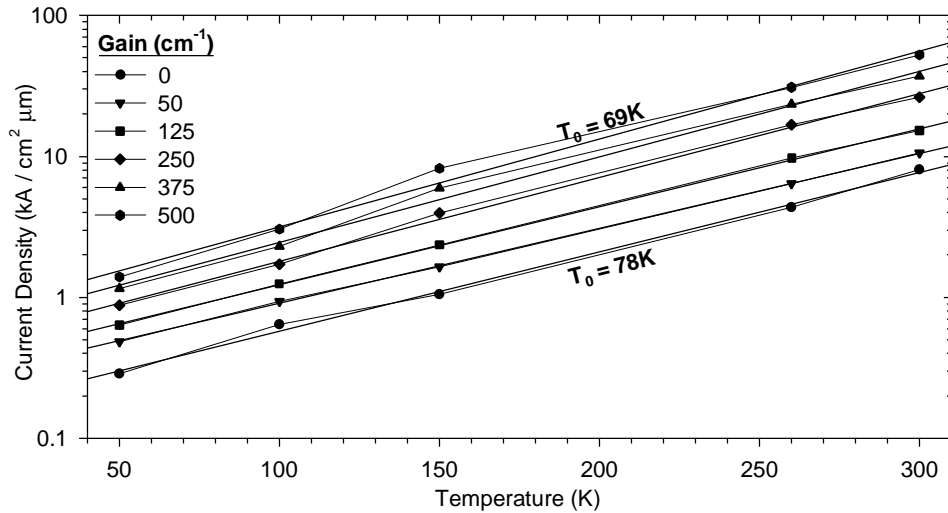


Figure 5: Injected carrier densities as a function of lattice temperature for different amounts of gain.

temperature Auger coefficient and the large characteristic temperature are a direct consequence of the optimization of the band structure of this superlattice.

ACKNOWLEDGMENTS

This research was supported in part by the U.S. Air Force, Air Force Materiel Command, Phillips Laboratory (PL), Kirtland AFB, NM 87117-5777 (Contract No. F29601-97-C0041) and the National Science Foundation (Grant Nos. ECS-9406680 and ECS-97-07799).

REFERENCES

1. Michael E. Flatté, J. T. Olesberg, S. A. Anson, Thomas F. Boggess, T. C. Hasenberg, R. H. Miles, and C. H. Grein, *Appl. Phys. Lett.* **70**, 3212 (1997).
2. Michael E. Flatté, T. C. Hasenberg, J. T. Olesberg, S. A. Anson, Thomas F. Boggess, Chi Yan, and D. L. McDaniel, Jr., *Appl. Phys. Lett.* **71**, 3764 (1997).
3. S. W. McCahon, S. A. Anson, D.-J. Jang, M. E. Flatté, Thomas F. Boggess, D. H. Chow, T. C. Hasenberg, and C. H. Grein, *Appl. Phys. Lett.* **68**, 2135 (1996).
4. D.-J. Jang, J. T. Olesberg, M. E. Flatté, Thomas F. Boggess, and T. C. Hasenberg, *Appl. Phys. Lett.* **70**, 1125 (1997).
5. S. W. McCahon, S. A. Anson, D.-J. Jang, and Thomas F. Boggess, *Opt. Lett.* **20**, 2309 (1995).
6. The additional wavelength tuning range as compared to Ref. 5 is made possible in part by the use of a potassium-titanyl-arsenate (KTA) rather than potassium-titanyl-phosphate (KTP) for the nonlinear crystal in the optical parametric oscillator cavity.
7. K. L. Vodopyanov, H. Graener, C. C. Phillips, and T. J. Tate, *Phys. Rev. B* **46**, 13194 (1992).
8. V. Chazapis, H. A. Blom, K. L. Vodopyanov, A. G. Norman, and C. C. Phillips, *Phys. Rev. B* **52**, 2516 (1995).
9. See references contained in Ref. 1.
10. J. T. Olesberg, S. A. Anson, S. W. McCahon, Michael E. Flatté, Thomas F. Boggess, D. H. Chow, and T. C. Hasenberg, *Appl. Phys. Lett.* **72**, 229 (1998).